Journal of Materials Chemistry C

Accepted Manuscript

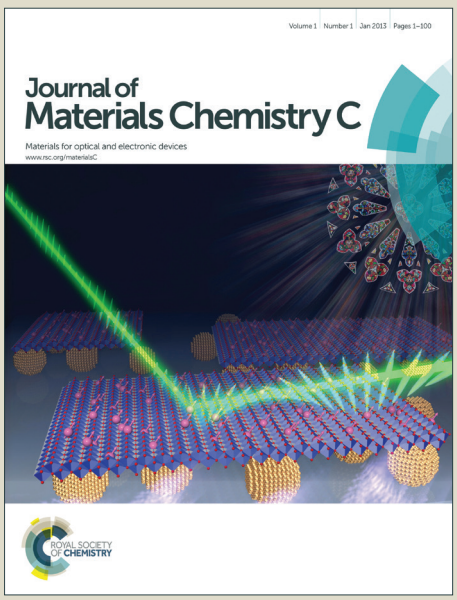

ROYAL SOCIETY OF CHEMISTRY

www.rsc.org/materialsC

Cite this: DOI: 10.1039/c0xx00000x

www.rsc.org/xxxxxx

ARTICLE TYPE

Columnar discotic Pt(II) metallomesogens as luminescence multifunctional materials with chemo and thermosensor abilities.

Cristián Cuerva,[a] José A. Campo,[a] Paloma Ovejero,[a] M. Rosario Torres,[b] Elisabete Oliveira,[c,d] Sérgio M. Santos,[e] Carlos Lodeiro[c,d] and Mercedes Cano*[a]

Received (in XXX, XXX) Xth XXXXXXXXX 20XX, Accepted Xth XXXXXXXXX 20XX
DOI: 10.1039/b000000x

A new family of Pt(II) luminescent metallomesogens based on dicatenar pyridylpyrazolate ligands $[Pt(pz^{R(n,n)py})_2]$ ($R(n,n) = C_6H_3(OC_nH_{2n+1})_2$, n = 4-18) has been prepared, and their mesomorphic and photophysical properties are described. The compounds were isolated as red (n = 4-8) or yellow (n = 10-18) solids at room temperature, but the first ones were converted to yellow crystals by slow evaporation of a chloroform-acetone mixed solution. All of them behave as discotic liquid crystal materials, exhibiting hexagonal columnar mesophases (Col_h) in a wide range of temperature. Photoluminescent studies in the solid state at variable temperature showed a high emission in the liquid crystalline phase, which was significantly red-shifted with respect to the yellow-green emission of the solid state. This photophysical change was attributed to the formation of aggregates through $Pt(d_z^2)$–$Pt(d_z^2)$ interactions, so giving rise to the metal-metal-to-ligand charge transfers (^{3}MMLCT) responsible for the luminescence observed. Taking advantage of these properties we have fabricated polymeric solid supports doped with the platinum complex $[Pt(pz^{R(10,10)py})_2]$, which can be used as temperature sensors for real technological applications. In addition, the Pt-bispyrazolate complexes and their corresponding pyrazole ligands have been proved to be useful as chemosensors towards Pd^{2+}, Zn^{2+}, Cd^{2+} and Hg^{2+} metal ions.

Keywords: Platinum complexes, discotic metallomesogens, sensor, luminescence

Introduction

Over the last years, the design of luminescent probes for application as chemosensors plays an important role in clinical medicine,[1,2] biology,[3-6] and environmental chemistry.[7-9] Recent research progress has been focused in the preparation of fluorescent chemosensors to selective detection and removal of heavy metal ions such as Cu^{2+}, Pd^{2+}, Zn^{2+}, Pb^{2+}, Cd^{2+} and Hg^{2+} which are highly harmful to both environment and human health.[10-12] Among them, mercury is one of the most pollutants and neurotoxic metals even at very low concentrations. Its presence in the human body can induce permanent brain damage to disrupt metabolic processes and cause depression or irritability. In the digestive tract, an acute poisoning by mercury can produce detachments of the gastrointestinal mucosa, resulting in a loss of fluids and electrolytes.[13] Therefore, it is evident the necessity to develop advanced materials and new methods for the analytical determination of these toxic metals.

On the other hand, the increasing utility of liquid crystal science to new technologies demands liquid crystalline materials that integrate novel structural elements and physical properties to be useful for their future applications. In this respect, discotic metallomesogens are of great interest[14] in fields such as optoelectronics (field-effect transistors, displays),[15,16] energy (solar cells)[17] or medicine (contrast agents).[18]

To these aims, Pt(II) complexes have been considered as an important topic due to their versatile physico-chemical properties. They have a d^8 electronic configuration which favours a square planar coordination geometry, giving rise to interesting luminescent and/or mesomorphic properties which are usually generated from stacking mode associated with intermolecular interactions, specially Pt-Pt and/or π-π ones.[19-27]

As a part of our research in metallomesogenic compounds formed by transition metal ions and pyrazole ligands,[28-30] we have recently reported discotic Pd(II) metallomesogens based on dicatenar pyridine-functionalised pyrazole ligands $[Pd(pz^{R(n,n)py})_2]$ and $[PdCl_2(Hpz^{R(n,n)py})]$ ($[Hpz^{R(n,n)py}]$ = 3-(3,5-bis(alkyloxy)phenyl)-(5-pyridin-2-yl)pyrazole, $R(n,n) = C_6H_3(OC_nH_{2n+1})_2$, n = 4, 6, 8, 10, 12, 14, 16, 18) which exhibited relevant columnar mesomorphism.[31]

Encouraged by our previous results, we were interested in extending the study to a new family of Pt(II) complexes based on these pyrazole ligands in order to obtain novel poly-functional molecular materials that combine both columnar liquid crystal and photoluminescence properties. In addition, taking advantage of the supramolecular organisation of the liquid crystals and their ease of processing, we have developed solid support sensors which can be used for real technological applications.

Table 1. Numbering of the compounds described in this work.

Compound	*n*	
[Hpz$^{R(n,n)py}$]	4	**a4**
	6	**a6**
	8	**a8**
	10	**a10**
	12	**a12**
	14	**a14**
	16	**a16**
	18	**a18**
[Pt(pz$^{R(n,n)py}$)$_2$]	4	**b4**
	6	**b6**
	8	**b8**
	10	**b10**
	12	**b12**
	14	**b14**
	16	**b16**
	18	**b18**

The synthesis and characterisation of the new platinum complexes, the establishment of their liquid crystalline and photoluminescent behaviour and their applications as temperature sensors and chemosensors for certain cations are discussed in this work.

The pyrazole ligands **a4-a18** previously reported by us[31] and the new Pt(II) compounds **b9-b18** described in this work are schematically presented in Table 1. The numbering used to identify them implies a letter to indicate the type of compound and a number corresponding to the carbon atoms number in the alkyl chain.

Results and discussion

Synthesis and characterisation

Bispyrazolate Pt(II) complexes [Pt(pz$^{R(n,n)py}$)$_2$] (R(*n*,*n*) = $C_6H_3(OC_nH_{2n+1})_2$; *n* = 4, 6, 8, 10, 12, 14, 16, 18) **b4-b18** were synthesized by reaction of the corresponding dicatenar pyrazole ligands [Hpz$^{R(n,n)py}$] **a4-a18** with K_2PtCl_4 in a 2:1 molar ratio (Scheme 1). The new compounds were isolated as red (*n* = 4-8) or yellow (*n* = 10-18) solids at room temperature, some of them containing molecules of water of solvatation. The first red complexes were transformed to yellow crystals from a chloroform-acetone mixed solution. This difference of colour will be justified later and will constitute the basis for their application as temperature sensors.

All complexes were fully characterised by spectroscopic techniques (IR, ^{1}H NMR and ^{13}C NMR in a selected case) and CHN elemental analysis (see experimental section). Single crystal X-ray structural analysis of **b8**, as a representative example of the obtained complexes, was also carried out in order to establish the potential structural relationship between the mesophase and the solid state.

The IR spectra of all complexes in the solid state show, among others, the characteristic ν(C=N) and ν(C=C) bands of the pyridine and pyrazole groups around 1597 cm^{-1}, slightly shifted at higher frequencies with respect to those of the free ligands. In addition, the band at *ca*. 765 cm^{-1} associated with the γ(CH) deformation of the pyridyl substituent was batochromically shifted.[31] These results, combined with the absence of ν(NH) vibrations in the higher-energy region, are consistent with the coordination of the ligand in its pyrazolate form.

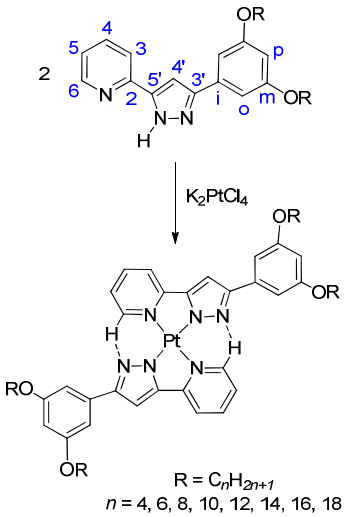

Scheme 1. Synthesis of the platinum complexes [Pt(pz$^{R(n,n)py}$)$_2$] **b4-b18**

On the other hand, the strong ν(CH) bands corresponding to the symmetric and antisymmetric stretches of the alkyl chains can be clearly observed in the range of 2848-2957 cm^{-1}. It is interesting to note that the position of these bands can be related with the order in the alkyl chains.[32] So, for complexes **b4** and **b6**, they appear 15-35 cm^{-1} at higher frequencies than for the remaining Pt(II) compounds, this shift suggesting that the compounds with short alkyl chains show a liquid-like order, while long chains produce a more crystalline order.

The ^{1}H NMR spectra in $CDCl_3$ solution at room temperature of all complexes and the ^{13}C NMR spectrum of **b12** as a representative example display the expected signals from the pyrazole ring and their substituent groups, which are shifted due to the coordination. The presence of only one set of signals for each type of protons or carbons is indicative of a high symmetry between the two pyridylpyrazolate ligands.

In particular, the signal from the 6-H proton of the pyridine group, which can be clearly observed at *ca*. 10.75 ppm, is downfield shifted in relation to that of the free ligand (*ca*. 8.64 ppm).[31] This fact is probably associated to the presence of intramolecular C–H···N hydrogen bonds (see below),confirming once again the anionic nature of the coordinated ligands.

Crystal structure of [Pt(pz$^{R(8,8)py}$)$_2$] b8

Suitable yellow crystals of **b8** were obtained by slow vapour diffusion of acetone into a chloroform solution of the complex. The compound crystallises in the triclinic space group *P*(-1), with two formula units per unit cell. The molecular structure is depicted in Figure 1, and Table S1 lists selected bond distances and angles.

The platinum atom is surrounded by four nitrogen atoms of the two pyridylpyrazolate ligands, giving rise to a square-planar geometry with mean Pt–N(pyrazole) and Pt–N(pyridine) distances of 1.98(1) and 2.03(1) Å, respectively. The environment

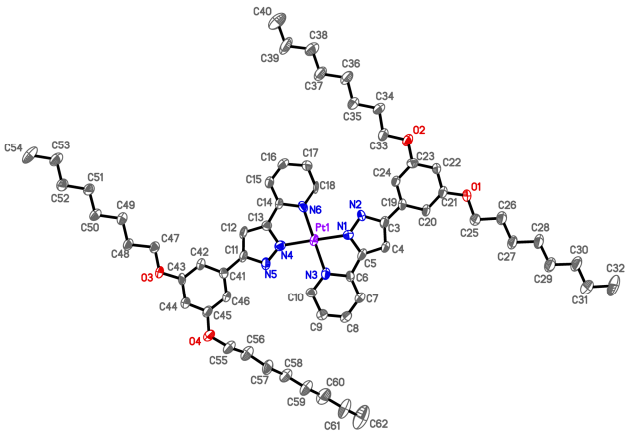

Figure 1. ORTEP plot for **b8** with 30% probability. Hydrogen atoms have been omitted for clarity. The inset shows the intramolecular hydrogen bonds between the pyrazolate ligands.

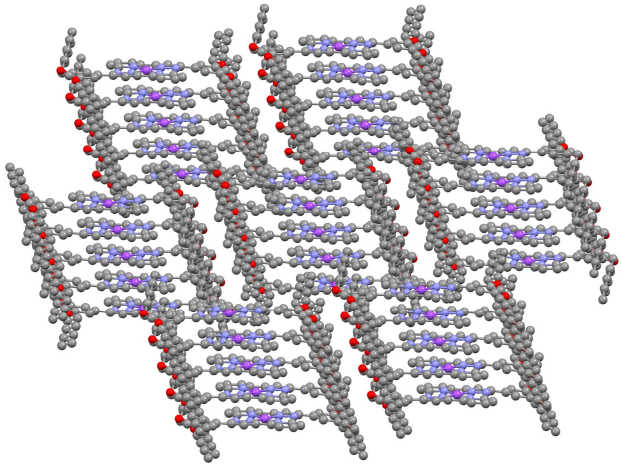

Figure 2. Columnar packing of **b8** through the *a* axis

around the metal centre presents a high planarity, as deduced from the two five-membered chelate rings originated from the Pt–N bonds, PtN1C5C6N3 and PtN4C13C14N6 (dihedral angle of 0.6(1)º). The major deviation of the square-planar geometry is produced from the bite angles of 79.6(4) and 80.8(4)º defined by the N1–Pt–N3 and N4–Pt–N6 bonds, respectively. In addition, the pyridine and benzene planes of each ligand are almost parallel with the own pyrazolate one (dihedral angles varying from 1.7 to 6.9(1)º).

As it can be observed in the inset of the Figure 1, the high planarity of the core combined with the anionic nature of the ligand favours the formation of intramolecular C–H···N hydrogen bonds between the non-coordinated N-pyrazolic and the nearest carbon atom from the pyridine group of the other ligand (d(C10···N5): 3.11(1) Å, <(C10–H10···N5): 143.4º; d(C18···N2): 3.07(1) Å, <(C18–H18···N2): 144.6º). Note that the strength of these bonds is comparable with that of the intermolecular N–H···N hydrogen bonds established in the free ligand.[31] In fact, they are maintained in solution as it can be deduced from the notable chemical shift observed for the 6-H pyridine proton in the ^{1}H NMR spectra of the complexes.

The C(pyrazole)-C(pyridine or benzene) distances of *ca*. 1.43 Å are, in general, slightly shorter than those found in the free ligand, this feature suggesting an higher delocalisation of the π electronic charge due to an increasing conjugation in the platinum complexes.

Table 2. Thermal behaviour of Pt(II) compounds

	n	Transition[a]	T[b] / ºC	ΔH / kJmol^{-1}
b4	4	Cr→Cr'→Col$_h$	146[c]	35.3
		Col$_h$→I	307[d]	
		I→Col$_h$	305[d]	
		Col$_h$→Cr	129	-6.0
b6	6	Cr→Cr'→Col$_h$	107[c]	51.1
		Col$_h$→I	251	1.2
		I→Col$_h$	242	-0.6
		Col$_h$→Cr	105	-7.0
b8	8	Cr→Cr'→Col$_h$	107[c]	17.1
		Col$_h$→I	248	1.8
		I→Col$_h$	241	-0.6
		Col$_h$→Cr	89	-1.2
b10	10	Cr→Cr'	80	
		Cr'→Col$_h$	83	78.9[c]
		Col$_h$→I	243	0.5
		I→Col$_h$	241	-1.0
		Col$_h$→Cr	73	-1.5
b12	12	Cr→Cr'→Col$_h$	94[c]	105.8
		Col$_h$→I	225[d]	
		I→Col$_h$	208	-0.4
		Col$_h$→Cr	69	-3.8
b14	14	Cr→Cr'	81	5.3[e]
		Cr'→Col$_h$	94	93.6
		Col$_h$→I	211[d]	
		I→Col$_h$	203[d]	
		Col$_h$→Cr	80[d]	
b16	16	Cr→Cr'	99	
		Cr'→Col$_h$	102	117.2[c]
		Col$_h$→I	193[d]	
		I→Col$_h$	192[d]	
		Col$_h$→Cr	90[d]	
b18	18	Cr→Cr'	104	
		Cr'→Col$_h$	107	176.8[c]
		Col$_h$→I	149[d]	
		I→Col$_h$	138[d]	
		Col$_h$→Cr	90[d]	

[a] Cr, Cr' = crystalline phases, Col$_h$ = hexagonal columnar mesophase, I = isotropic liquid. [b] DSC onset peaks. [c] Overlapped processes. [d] Detected by POM. [e] ΔH(exothermic peak at 83 ºC) = -15.0 kJmol^{-1}

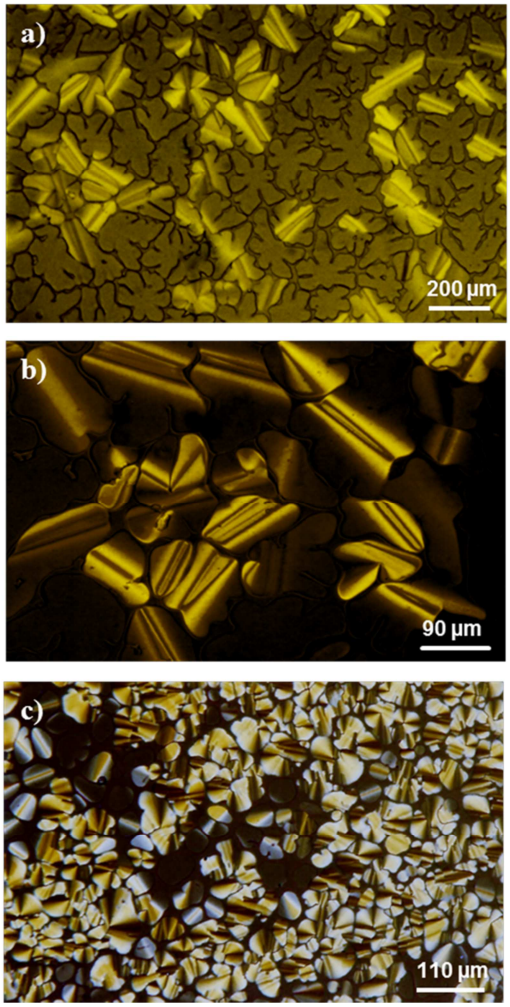

Figure 3. Microphotographs of **(a, b)** [Pt($pz^{R(12,12)py}$)$_2$] **b12** at 207 ºC and 190 ºC, respectively, and **(c)** [Pt($pz^{R(18,18)py}$)$_2$] **b18** at 119 ºC, on cooling.

On the other hand, each molecular unit shows a disc-like shape in which the two alkyl chains of each ligand are almost coplanar with the benzene rings, as deduced from the angles between the lines linking the oxygen and the terminal carbon atoms at each chain and the normal to the own benzene plane which range from 74.9 to 87.8(1)º. In this arrangement, the four alkyl chains run almost parallel and they are extended *ca*. 10 Å (mean value measured as the distance between the oxygen and the terminal carbon atoms at each chain), exhibiting an extensive interdigitation with the terminal chains of neighbouring molecules (see Figure S1).

On a supramolecular level, weak $\pi\cdots\pi$ interactions of *ca*. 3.4 Å defined between the pyridine and benzene rings give rise to a columnar packing of molecules along to the *a* axis. Note that the core is rotated *ca*. 40º with respect to the axis defined by the platinum atoms. In this situation, the platinum centres are located at 6.71(1) Å (Figure 2).

Mesomorphic behaviour

The thermal behaviour of the new Pt(II) compounds has been examined by using both polarised optical microscopy (POM) and differential scanning calorimetry (DSC) techniques. Additionally, an X-ray diffraction study at variable temperature was also performed for **b12** in order to confirm the nature of the mesophases. Table 2 lists the phase transition temperatures and their associated enthalpy data established by DSC.

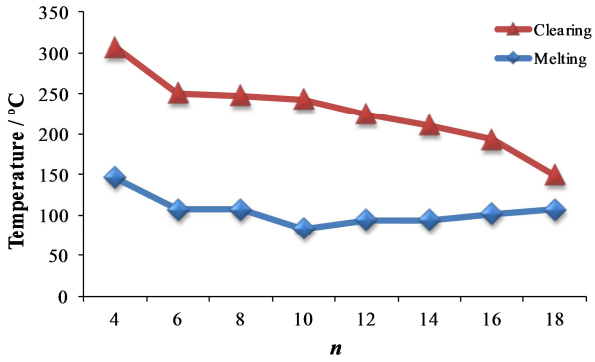

Figure 4. Melting X-Rayd clearing temperature-*n* graph of Pt(II) complexes

All platinum complexes exhibited enantiotropic mesomorphism showing columnar phases as expected for disc-like molecules. The mesophases were undoubtedly identified as Col_h on the basis of their pseudo focal-conic and dendritic textures, which were observed during the cooling process from the isotropic liquid (Figure 3). The presence of homeotropic domains was consistent with the preferred uniaxial character[33] of the columnar phases.

The DSC thermograms exhibited a different pattern as a function of the length of the terminal alkyl chains. In the case of the platinum complexes bearing chains with $n < 14$ carbon atoms, endothermic peaks assigned to solid-solid, solid-mesophase and mesophase-isotrope transitions could be observed during the first heating, the two first transitions usually overlapping in a single peak. Note that the solid-solid transformation was not observed in the successive cycles of heating, which suggests that this structural change occurs irreversibly. On cooling from the isotropic liquid, exothermic peaks were detected at temperatures similar to those measured on heating (except the isotrope-mesophase transition of **b4**), in agreement with the formation of the mesophase and the solidification process.

By contrast, DSC traces of the complexes with longer side chains (n = 14, 16 and 18) did not show the peak corresponding to the clearing temperature. Likewise, on cooling the formation of the mesophase from the isotropic liquid could not be observed, so that the temperatures of these phase transitions were determined by POM. The absence of these peaks in the DSC thermograms can suggest that these Col_h phases are highly disordered,[34] probably due to the increase of the alkyl chains length.

In general terms, in the first cycle of heating the solid-solid and the solid-mesophase transitions occur at temperatures very close to each other, appearing practically overlapped as previously commented. However, in the particular case of **b14** the two peaks corresponding to these phase transitions were separated by 13 ºC, which allowed to observe an intermediate exothermic peak (ΔH = -15.0 kJmol^{-1}) at 83 ºC on the first heating. This fact can be attributed to the formation of Pt-Pt interactions between molecules in the solid which should favour the attainment of the columnar mesophase, as it has been previously suggested from similar results reported in the literature.[31]

Table 3. Absorption (λ_{abs}^{max}) and emission (λ_{em}^{max}, $\lambda_{em\,(solid)}^{max}$) maxima in nm, molar absorption coefficients (ε) in $Lmol^{-1}cm^{-1}$ and luminescence quantum yields (Φ_F) for ligands and complexes in CH_2Cl_2 solution and in the solid state at 298 K

Compound	*n*		λ_{abs}^{max} ($\varepsilon/10^4$) [a]	λ_{em}^{max} [a]	$\lambda_{em\,(solid)}^{max}$ [a]	$\Delta\lambda$ [b]	Φ_F [c]
$[Hpz^{R(n,n)py}]$	6	**a6**	258 (1.7), 286(1.0)	374	365	88	0.04
	10	**a10**	258 (2.2), 286 (1.5)	374	364	88	0.03
	12	**a12**	258 (1.8), 286 (1.2)	374	365	88	0.04
	18	**a18**	258 (2.0), 286 (1.3)	374	365	88	0.04
$[Pt(pz^{R(n,n)py})_2]$	4	**b4**	270 (7.8), 340 (2.7), 436 (0.6)	500	504, 533	64	0.01
	6	**b6**	271 (5.5), 299 (4.8), 436 (0.4)	500	500, 532	64	0.01
	8	**b8**	270 (7.4), 340 (2.7), 436 (0.5)	500	505, 533	64	0.01
	10	**b10**	270 (6.0), 340 (2.4), 435 (0.4)	500	506, 531	65	0.01
	12	**b12**	276 (2.5), 342 (0.9), 436 (0.1)	500	505, 531	64	0.02
	14	**b14**	269 (13.2), 340 (5.4), 434 (0.1)	500	500, 535	66	0.01
$[Pd(pz^{R(n,n)py})_2]$	6	**c6**	272 (1.7), 296 (1.5), 325 (sh) (0.7)	375	-	50	<0.01
	12	**c12**	272 (5.5), 296 (4.8), 325 (sh) (2.6)	376	-	51	<0.01
$[PdCl_2(Hpz^{R(n,n)py})]$	6	**d6**	266 (1.8), 300 (1.6), 300 (1.4)	360	-	60	<0.01
	18	**d18**	266 (2.7), 300 (2.5), 298 (2.1)	360	-	62	<0.01

[a] Estimated error: ± 1 nm. [b] Stokes shift. [c] Estimated error: ± 5 %. (sh = shoulder)

A comparative study of the melting and clearing temperatures of all platinum metallomesogens shows the great influence of the alkyl chain length on the mesomorphic properties (Figure 4). In compounds with short alkyl chains (n < 10) the melting temperatures decrease by increasing the chain length, favouring the formation of the mesophase. However, when the number of carbon atoms is greater than 10 at the hydrophobic chains, an increase of the melting temperatures is observed by increasing of n, so indicating that the van der Waals interactions among the hydrophobic tails in the solid are a determinant factor. In all cases, the clearing temperature decreases by increasing the chain length, so that shorter alkyl chains give wider mesophase stability ranges. Thus, the complex with four carbon atoms exhibits a very high clearing temperature and shows the highest stability interval.

In order to confirm the columnar nature of the liquid crystal phases, the compound **b12**, selected as a representative example, was subjected to temperature-dependent powder X-ray diffraction (XRD) measurements. As it can be observed in Figure S2, the 2D XRD patterns at the mesophase temperature showed four peaks in the small angle region with a d-spacing ratio of 1: $1/\sqrt{3}$: $1/\sqrt{4}$: $1/\sqrt{7}$, which were indexed as (100), (110), (200) and (210) reflections of a two-dimensional hexagonal lattice (a = 27 Å).[35]

The maximum corresponding to the intracolumnar distance was not observed in any of the diffractograms registered during the range of existence of the mesophase, which is indicative of a high disorder along each column[36] in agreement with the small enthalpy values associated to the clearing process. In this situation, the relationship between the molecular volume V_m (2073 $Å^3$) and the columnar cross-section area S_{col} (631 $Å^2$)[‡] was *ca*. 3.3 Å. This value is usually found for the (001) reflection corresponding to the stacking distance, so that taking into account the relationship $cS_{col} = ZV_m$, in which Z is the number of molecules per columnar unit, it is deduced that a single Pt(II)

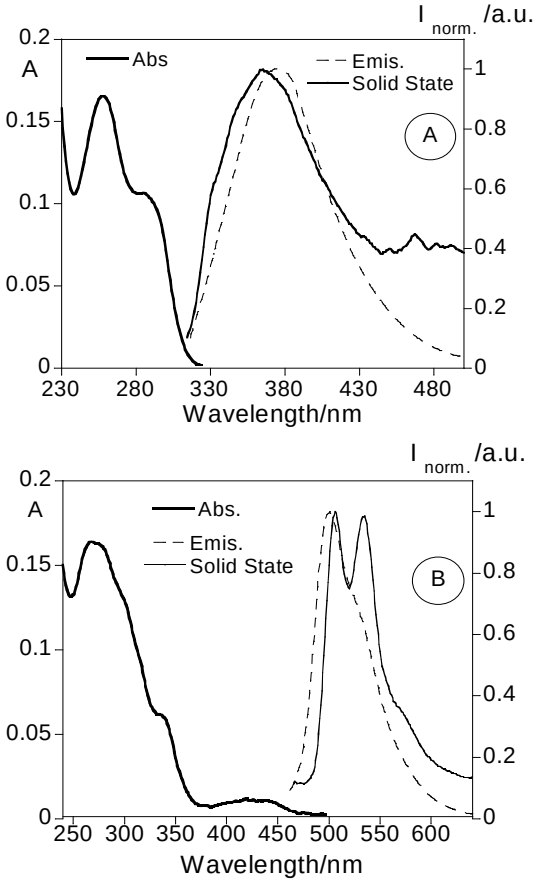

Figure 5. Absorption (bold full line), emission (broken line) in CH_2Cl_2 solution (1×10^{-5} M) and emission at solid state (full line) spectra of $[Hpz^{R(6,6)py}]$ **a6** (A) and of $[Pt(pz^{R(8,8)py})_2]$ **b8** (B) at room temperature (λ_{exc} = 286 nm for **a6**, λ_{exc} = 340 nm for **b8**).

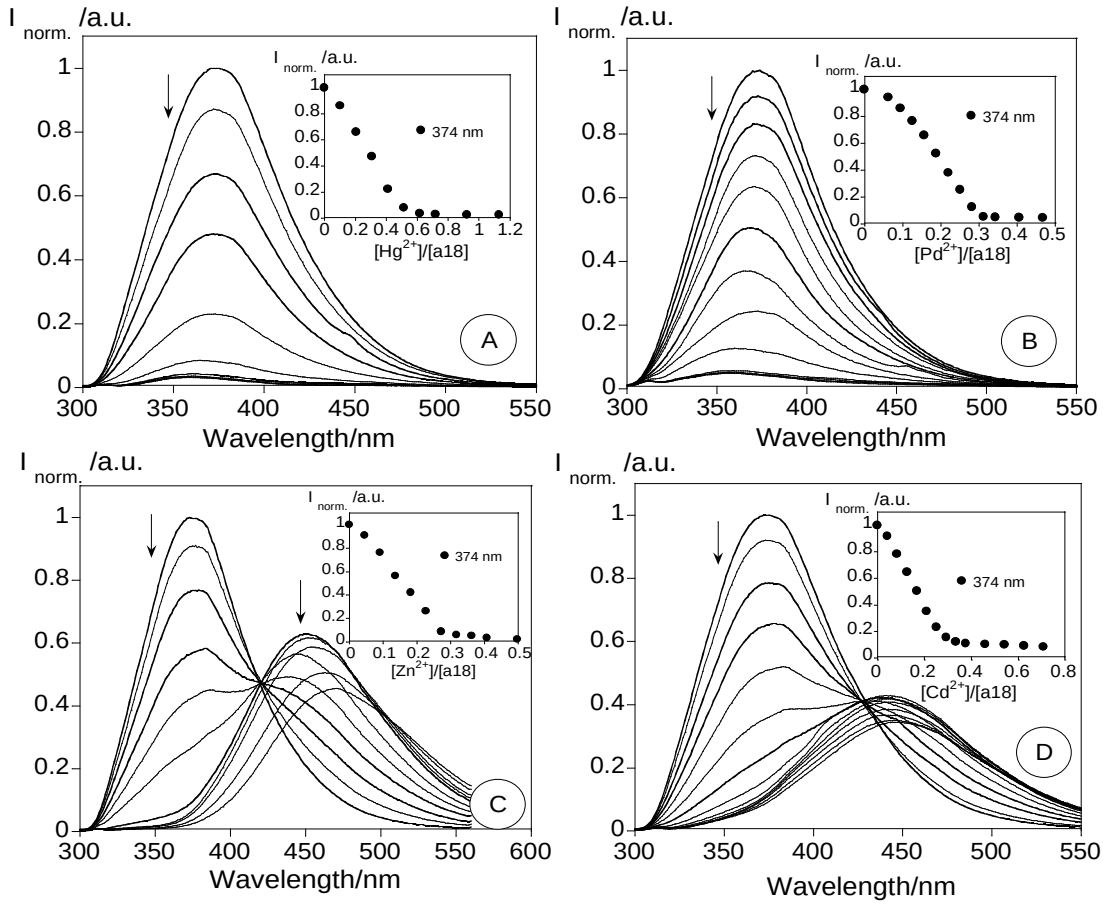

Figure 6. Normalised fluorescence titrations for [$Hpz^{R(18,18)py}$] **a18** in CH_2Cl_2 solution (1 x 10^{-5} M, λ_{exc} = 286 nm) as a function of increasing amounts of $Hg(NO_3)_2$ (A), $[Pd(CH_3CN)_4][BF_4]_2$ (B), $Zn(BF_4)_2$ (C) and $Cd(CF_3SO_3)_2$ (D). Insets show the emission read as a function of $[Hg^{2+}]/[$**a18**$]$ (A), $[Pd^{2+}]/[$**a18**$]$ (B), $[Zn^{2+}]/[$**a18**$]$ (C) and $[Cd^{2+}]/[$**a18**$]$ (D).

complex occupies the cross-section area of an elementary discotic unit.

On the other hand, the absence of the characteristic broad halo corresponding to the liquid-like arrangement of the alkyl chains is probably due to this lack of short-range order.

Photophysical Characterisation

The absorption, emission and excitation spectra of the polycatenar pyrazole ligands **a6, a10, a12, a18** and their corresponding Pt(II)-bispyrazolate complexes **b4**-**b18** were measured in dichloromethane solutions (*ca*. 10^{-5}-10^{-6} M) and in the solid state at 298 K. Similar spectrophotometric and spectrofluorimetric studies for analogous Pd(II) metallomesogens **c6**, **c12**, **d6** and **d18**, which have been recently reported by us,[31] were also carried out for comparison. As a representative example, Figure 5 shows the photophysical characterisation of the pyrazole ligand [$Hpz^{R(6,6)py}$] **a6** and the complex [$Pt(pz^{R(8,8)py})_2$] **b8**, respectively. All results are summarised in Table 3.

Pyrazole ligands (**a6**, **a10**, **a12**, **a18)** exhibit a broad absorption band in the region of 250-290 nm attributed to the π-π* transitions of pyrazole and/or pyridine units,[29] with the maximum at 258 nm and a shoulder at 286 nm. Concerning the emission spectra, a band with a maximum centred at 374 nm was observed, with a similar fluorescence quantum yield of *ca*. 0.03-0.04. In all cases, these emission bands are slightly red-shifted with respect to ones observed in the solid state. Taking into account these results, it is important to indicate that the increasing number of carbon atoms does not significantly affect the photophysical spectral behaviour.

The absorption spectra of Pt(II) complexes (**b4**-**b14**) show three bands. The two first, at 269-276 nm and at 340 nm respectively, correspond to characteristic electronic transitions of the organic ligands, which are red-shifted to respect to the free ligands and exhibit higher molar absorptions coefficients ranging between 0.9-13.2×10^4 $Lmol^{-1}cm^{-1}$. The third band, observed in a lower-energy region at *ca*. 436 nm ($\varepsilon \approx 10^3$ $Lmol^{-1}cm^{-1}$), was attributed to a metal-to-ligand charge transfer (MLCT) in both the singlet and triplet manifolds.

The luminescence spectra in solution and in the solid state display emission bands originated from Pt(II) monomer units which are bathochromically-shifted with respect to these of the corresponding pyrazole ligand, exhibiting a Stokes shift of *ca*. 64 nm. Particularly, in the solid state appears a second intense fluorescence band which was red-shifted (λ_{em} = 531-535 nm) related to that of the solution (λ_{em} = 500 nm). It is interesting to note that the origin of this shift could be attributed to the presence of $\pi \cdots \pi$ interactions between the pyridine and benzene rings of neighbouring monomers, which do not exist in solution.[22] The fluorescent nature at room temperature of the yellow Pt(II) derivatives was evidenced from the lifetime of complex **b12** (4.5 ns), selected as a representative example.

Table 4. Stability constants for ligands **a6** and **a18** in CH_2Cl_2 in the presence of Zn^{2+}, Cd^{2+}, Hg^{2+} and Pd^{2+} and Pt(II) complexes **b6** and **b14** in CH_2Cl_2 in the presence of Hg^{2+}.

Compound	Interaction	∑logβ (emission)
a6	Zn^{2+} (3:1)	17.56±0.01
	Cd^{2+} (3:1)	17.57±0.01
	Hg^{2+} (2:1)	12.52±0.03
	Pd^{2+} (3:1)	18.21±0.07
a18	Zn^{2+} (3:1)	17.55±0.09
	Cd^{2+} (3:1)	17.51±0.04
	Hg^{2+} (2:1)	15.52±0.13
	Pd^{2+} (3:1)	20.35±0.04
b6	Hg^{2+} (1:1)	6.61±0.01
b14	Hg^{2+} (1:1)	6.85±0.01

To a comparative purpose, similar studies were carried out for the palladium compounds $[Pd(pz^{R(n,n)py})_2]$ (n = 6,12) **c6, c12** and $[PdCl_2(Hpz^{R(n,n)py})]$ (n = 6, 18) **d6, d18**. In general terms, the most significant differences with respect to the spectra of the Pt(II) complexes were related with the shift of the fluorescence bands to a lower wavelength and with the absence of emission in the solid state. The fluorescent quantum yield was also affected by the metal showing the strongest values for platinum derivatives.

Sensorial ability towards metal ions

In order to explore the potential sensorial ability of the pyrazole ligands and their corresponding platinum derivatives, several metal titrations followed by absorption and emission measurements were performed in dichloromethane solution with the addition of different metal salts in acetonitrile.

The fluorescence response of **a6** and **a18**, chosen as representative examples of the ligands, was tested towards the soft metal ions Hg^{2+}, Pd^{2+}, Zn^{2+} and Cd^{2+}. A similar behaviour was observed in both compounds, and therefore in Figure 6 are only depicted the titration spectra of **a18**. As it can be observed, the natural fluorescence emission of the pyrazoles is strongly quenched by addition of increasing amounts of Hg^{2+} and Pd^{2+}, which is consistent with the chelation enhancement of the quenching effect (CHEQ).[37-39]

In the case of the addition of Hg^{2+}, a total quenching of the emission band was observed upon the addition of half metal equivalent, while only 0.3 equivalents of Pd^{2+} were necessary to achieve a similar quenching effect (insets of Figure 6A,B).

A different behaviour was observed upon Zn^{2+} and Cd^{2+} complexation. In both cases, the emission band of the free ligand centred at 374 nm was quenched, but at the same time a new red-shifted emission was turning up at *ca*. 447 nm. The plateau observed in the insets of Figure 6C,D after addition of *ca*. 0.3 equivalents of metal ion suggests the formation of complexes with a 3:1 (ligand-to-metal) molar ratio.

On the other hand, no significant changes were detected in absorption spectra, verifying only a small decrease of the band centred at 258 nm (see Figure S3).

In order to postulate the stoichiometry of the metal complexes formed in solution from the ligands, the stability constants were determined using the HypSpec program[40] and are gathered in Table 4. The results suggest the formation of complexes with a 3:1 ligand-to-metal stoichiometry for the interaction of ligands **a6** and **a18** with Zn^{2+}, Cd^{2+} and Pd^{2+}, while a 2:1 ligand-to-metal

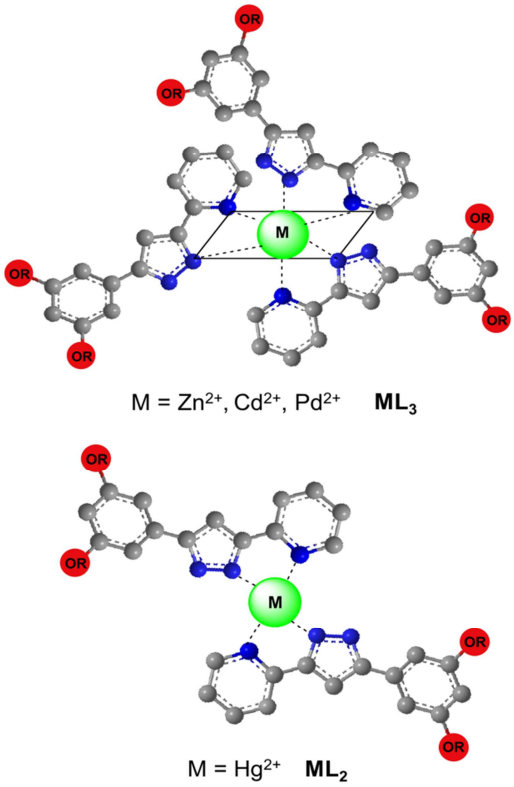

Figure 7. Schematic representation of coordination mode for ML_3 and ML_2 complexes (R = C_6H_{13} or $C_{18}H_{37}$).

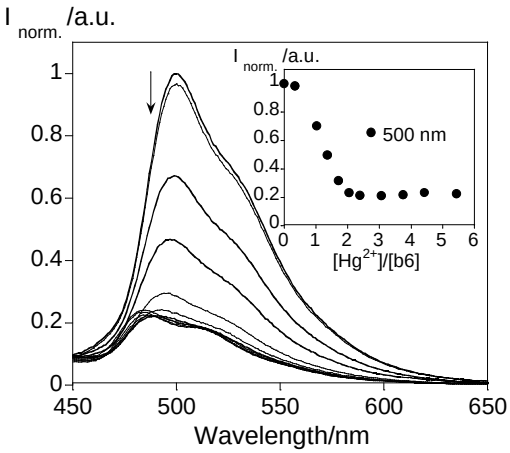

Figure 8. Normalised fluorescence titrations for $[Pt(pz^{R(6,6)py}]$ **b6** in CH_2Cl_2 solution (5 x 10^{-6} M) as a function of increasing amounts of $Hg(NO_3)_2$. The inset shows the emission read at 500 nm as a function of $[Hg^{2+}]$/[**b6**].

molar ratio was deduced for the complexes obtained from the titrations with Hg^{2+}. These features point out to a bidentate coordination of ligands through of pyrazole and pyridine nitrogens to the metal ion, giving rise to six (Zn^{2+}, Cd^{2+} and Pd^{2+}) and four (Hg^{2+}) coordination environments in agreement with the structures suggested in Figure 7. Careful inspection of the stability constant values indicated that the strongest interaction was observed for Pd^{2+} with a value of logβ = 18.21±0.07 for **a6** and logβ = 20.35±0.04 for **a18**. Both ligand-to-metal stoichiometries, 2:1 and 3:1, were also confirmed on the basis of the Job's plot method.[41]

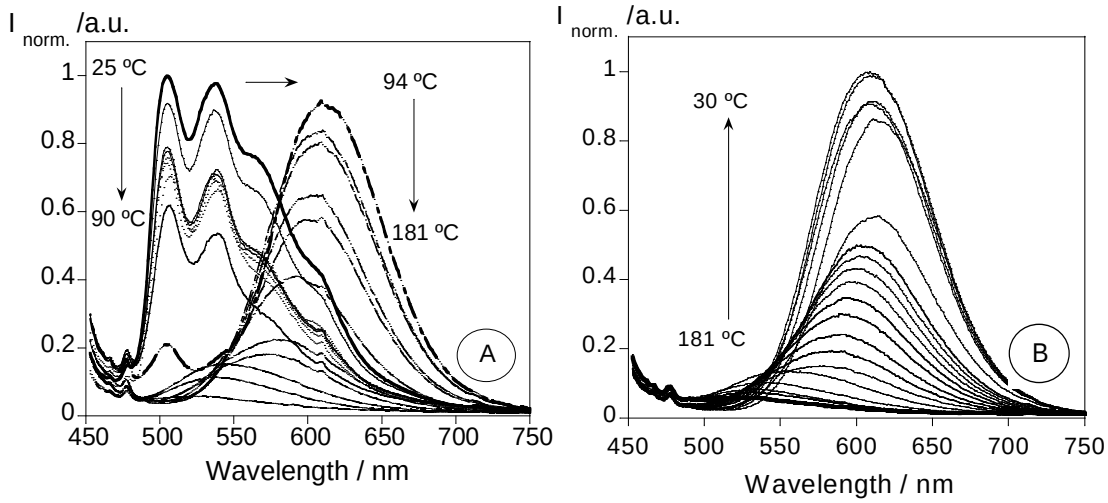

Figure 9. Fluorescence spectra of Pt(II) complex **b12** in the solid state as a function of temperature on heating (A) and on cooling (B).

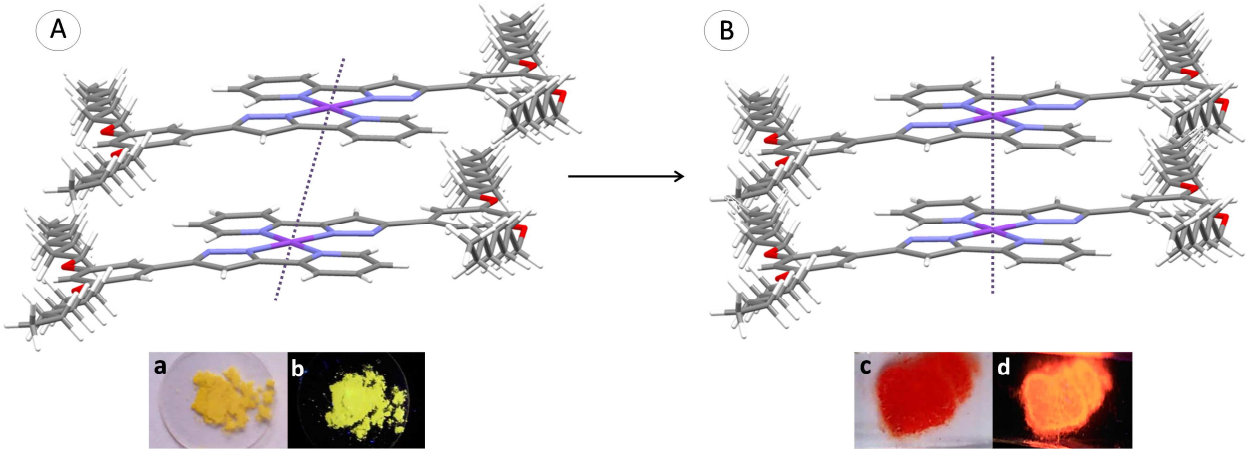

Figure 10. (A,B) Solid-solid transformation for Pt(II) complexes on heating. The insets show images of **b12** in the solid state at 25 ºC (a,b) and in the mesophase at 94ºC (c,d) taken with the naked-eye (left) and under UV lamp (λ_{exc} = 365 nm) (right).

On the other hand, the fluorescence behaviour of Pt(II) complexes towards different drugs (caffeine, nicotine, ibuprofen) and ions (CN^-, I^-, Hg^{2+}) was also investigated. Among the various species tested only the addition of Hg^{2+} caused a remarkable change in the natural emission band of **b6** and **b14**, selected as representative examples. In both cases, the fluorescence maximum centred at 500 nm was decreasing upon successive addition of Hg^{2+}, according to the expected CHEQ effect. However, unlike the free ligands, a total quenching was not produced. After adding 2 equivalents of Hg^{2+}, the fluorescence intensity remained constant as it is observed in Figure 8.

On the other hand, the stability constants were also calculated obtaining values of logβ = 6.61±0.01 for **b6** and of logβ = 6.85±0.01 for **b14** (Table 4), both of them revealing a 1:1 complex-to-metal stoichiometry.

At the same time, in both cases explored, the absorption spectra do not show significant changes.

Variable temperature luminescence studies

The photophysical properties of the pyrazole ligand **a6** and Pt(II) complexes **b4-b14** were studied at different temperatures from the solid to the liquid crystal states on heating and from the mesophase to the solidification process on cooling.

The emission band in solid state of the dicatenar pyrazole **a6** (see Figure S4) centred at 365 nm is almost unaffected until *ca.* 46 ºC, when a strong quenching was observed. From this temperature the fluorescence maximum was blue-shifted from 365 nm to 340 nm ($\Delta\lambda$ = 25 nm) in the heating cycle, indicating that the excited state is slightly modified. The photophysical behaviour was not restored on cooling.

However, several remarkable and very interesting changes in the photoluminescence of the Pt(II) compounds were observed by variation of the temperature. The luminescence spectra of complex **b12** as a representative example are shown in Figure 9.

On heating, from room temperature until *ca.* 90 ºC, the behaviour of the emission band at 505 nm is similar to that reported for other platinum complexes, showing a slow decrease of the fluorescence intensity by increasing temperature.[22,42] At the same time, a new red-shifted emission band (λ_{em} = 605 nm) arose at 94 ºC with a similar luminescence intensity to that of the initial solid, which gradually is blue-shifted and decreases in intensity upon the temperature increases. This peculiar red-shift from emission maximum is indicative of a structural change in the solid state which clearly affects the excited state. As it is known,

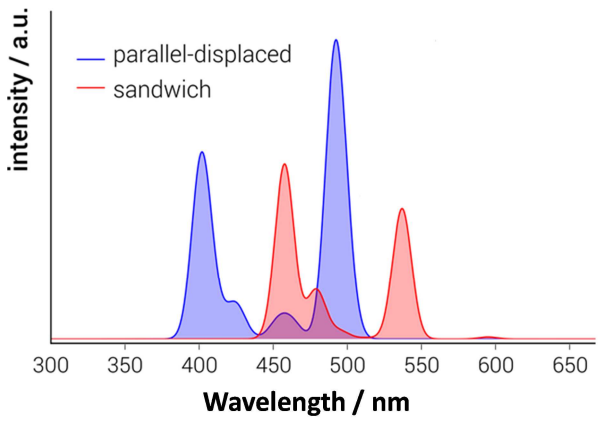

Figure 11. Simulated fluorescence spectra calculated with the TDDFT formalism at the B3LYP/LanL2DZ level. The TD spectra were simulated by fitting lorentzian functions (FWHM=15 nm), centred at the calculated excitation wavelengths.

the square-planar geometry of d^8-metal complexes allows the formation of aggregates through axial interactions.[43-45] On this basis, the new emissive red-shifted band could be attributed to a triplet metal-metal-to-ligand charge transfer (^{3}MMLCT) state probably due to the formation of aggregates through Pt(d_z^2)–Pt(d_z^2) interactions, which should favour the supramolecular ordering of the Col_h mesophase observed (see Figure 10). The large Stokes shift of 169 nm and the lifetime (70 ns) of **b12** confirm the phosphorescent nature of solid state luminescence corresponding to the molecular aggregates.

In agreement with this fact, the DSC thermogram of **b12** shows an overlapped peak at 94 ºC corresponding to the above mentioned solid-solid and solid-mesophase transitions (Table 2). This red-shift could be also observed with a naked eye when the complexes were studied by POM.

On cooling, the emission from the mesophase is gradually recovered and the maximum remains at 605 nm when the solidification temperature is reached (Figure 9B). These results suggest that the solid-solid transformation observed on the first heating is not reversible, so that the molecular arrangement of the mesophase is maintained after the mesophase-solid transition.

The above results allow us to establish that the liquid crystal state not only does not quench the emission, but enhances it.

On the other hand, thin films were prepared by the dip-coating method from CH_2Cl_2 solutions of the yellow Pt(II) complexes. Interestingly, a strong red fluorescence could be immediately observed after evaporation of the solvent. Fluorescence spectra registered at room temperature show an intense emission band centred around 617 nm, which is attributed to the ^{3}MMLCT transition of the Pt(II) aggregates. These results suggest that the molecular arrangement adopted in thin layer is probably the same as that proposed in the mesophase. Likewise, the red colour of the complexes **b4-b8** obtained before crystallising also evidences the presence of Pt-Pt aggregates at room temperature.

DFT calculations

In order to ascertain the mechanism leading to the red-shifting of the absorption spectra of the Pt(II) complexes upon heating, time-dependent density functional theory (TDDFT) calculations were performed using Gaussian09,[46] at the B3LYP/LanL2DZ level.

Table 5. Calculated TDDFT singlet (S_n) and triplet (T_n) vertical excitation wavelengths (in nm) and corresponding singlet oscillator strengths (in parenthesis) for the parallel-displaced and sandwich conformations, as calculated at the B3LYP/LanL2DZ level.

Exc	T_n / nm[a]	S_n / nm[a]	T_n / nm[b]	S_n / nm[b]
1	542.65	498.10 (0.0114)	733.05	693.92 (0.0000)
2	537.01	491.16 (0.0357)	632.69	594.88 (0.0003)
3	491.85	462.63 (0.0023)	576.72	536.99 (0.0185)
4	482.84	453.40 (0.0025)	539.19	531.68 (0.0002)
5	460.05	429.45 (0.0006)	522.64	513.46 (0.0002)
6	449.66	424.05 (0.0046)	517.33	495.09 (0.0011)
7	440.97	410.60 (0.0014)	507.74	479.03 (0.0070)
8	435.61	408.21 (0.0030)	503.75	459.26 (0.0001)
9	415.07	401.57 (0.0103)	491.74	457.73 (0.0240)
10	410.24	401.04 (0.0141)	490.41	455.16 (0.0009)

[a] Parallel-displaced conformation. [b] Sandwich conformation

The mechanism being considered is that, upon heating of the solid, the unit cell deforms such that the two previously non-interacting metals from adjacent complexes suddenly become above each-other, leading to direct interaction between the d_z^2 orbitals of the metals and, thus, to a red-shift of the emission spectra. With the purpose of validating this mechanism, two dimmer configurations were considered: one taken directly from the X-ray determined structure (parallel-displaced conformation; see Figure S5) and another where one of the molecules was translated along its molecular plane as to place the two platinum atoms above each other (sandwich conformation; see Figure S6). In both structures, the aliphatic substituents were replaced with methyl fragments in order to reduce the computational cost of the calculations. The hydrogen positions were allowed to relax prior to the calculation of the vertical excitation energies, since these are known to be wrongly assigned in X-ray derived structures.

In Figure 11 are shown the simulated fluorescence spectra (*i.e.* S_n->S_0 transitions) of both conformations. The calculated red-shifting of *ca.* 60 nm when going from the parallel-displaced to the sandwich conformation is consistent with the shift observed experimentally, if the underlying mechanism would be fluorescence. Within that scenario, and in the case of the parallel-displaced conformation, the lowest energy vertical excitation, at 2.49 eV (498.1 nm), is a S_0->S_1 transition, mainly dominated by a HOMO->LUMO excitation. In the case of the sandwich conformation, the first non-zero oscillator strength excitation corresponds to a S_0->S_2 transition at 2.08 eV (594.9 nm), dominated by a HOMO-1->LUMO excitation (Figure 12). Interestingly, the LUMO is mainly localized in a single platinum atom in the parallel-displaced and absent in the second metal, whereas in the sandwich conformation it embraces both metals in a rather symmetric way. In fact, the LUMO in this conformation has major contributions from the d_z^2 atomic orbitals of the two metals, which implies a major contribution of the metal to the photophysical properties of the complex. However, experimental results suggest that phosphorescence is the mechanism beneath the emission spectrum of the sandwich conformation. In Table 5 are reported the wave lengths associated with the triplet excitations, for both conformations. Similarly to the singlet-singlet transitions, the phosporescence transitions (*i.e.* T_n->S_0) are characterised by a red-shift of the associated wavelengths upon moving from the displaced to the sandwich conformation (it should be noted that oscillator strengths were not calculated for

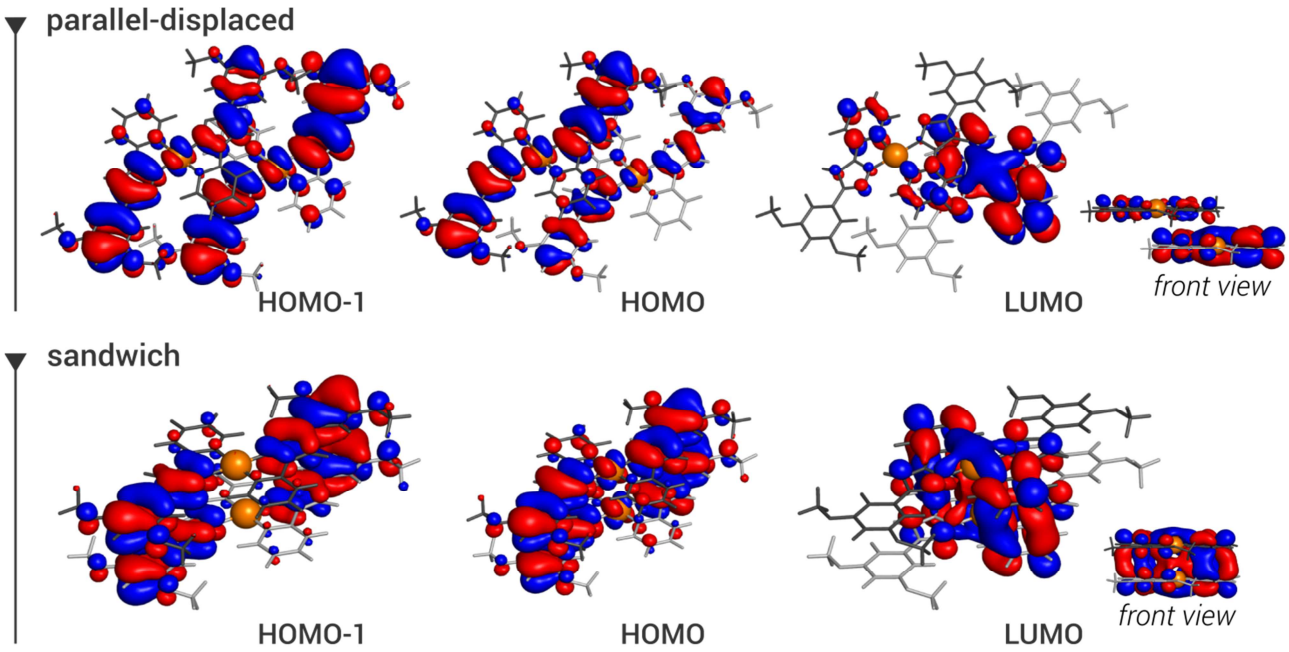

Figure 12. Principal molecular orbitals involved in the S_0->S_1 and S_0->T_1 (for the parallel-displaced conformation) and S_0->S_2 and S_0->T_2 (for the sandwich conformation) excitations, as calculated at the B3LYP/LanL2DZ. Platinum atoms shown as orange spheres; remaining atoms pertaining to distinct complexes coloured in different shades of grey for sake of clarity.

triplet->singlet transitions). The lowest energy excitation for the parallel-displaced conformation is at 2.28 eV (542.6 nm) and shifts to 1.96 eV (632.7 nm) in the sandwich conformation, in agreement with the emission maximum observed at 533 and 605 nm, respectively. In the former, the excitation is dominated by a HOMO-1->LUMO transition, whereas the latter it is dominated by a HOMO->LUMO transition (Figure 12). This reflects the importance of the Pt-Pt interaction in the sandwich conformation, along with the contribution of their d_z^2 atomic orbitals to the LUMO, suggesting that the spin forbidden singlet-triplet excitations are made possible due to the strong spin-orbit coupling of the metal centres.

Solid Support Sensors

Taking advantage of the physical and structural changes of these complexes by varying the temperature, their potentiality as solid supported sensors was evaluated by preparation of a low-cost polymethylmethacrylate (PMMA) polymer doped with the platinum complex **b10** (PMMA10). This polymer was submitted to three different conditions, such as, (i) hot air (37ºC, 50ºC and 60ºC), (ii) hot water (from 50ºC to 90ºC), (iii) heated from room temperature to 80ºC on a hot-plate, measuring the fluorescent emission in solid state with the fibre optic system connected to the Horiba J-Y Fluoromax-4.

Changes in the emission colour from yellow-green (505 nm) to red (605 nm) were only observed in the conditions (ii) and (iii) but at different temperatures (Figure 13). So, in hot water this variation started at 80ºC, while in contact with a hot surface the change was detected at lower temperature, starting at *ca.* 48ºC.

In this latter condition, platinum complexes could be really useful as a polymeric material implanted on mobile phones, tablets or notebooks in order to detect a prolonged exposure to high temperatures. The irreversibility of the colour transformation

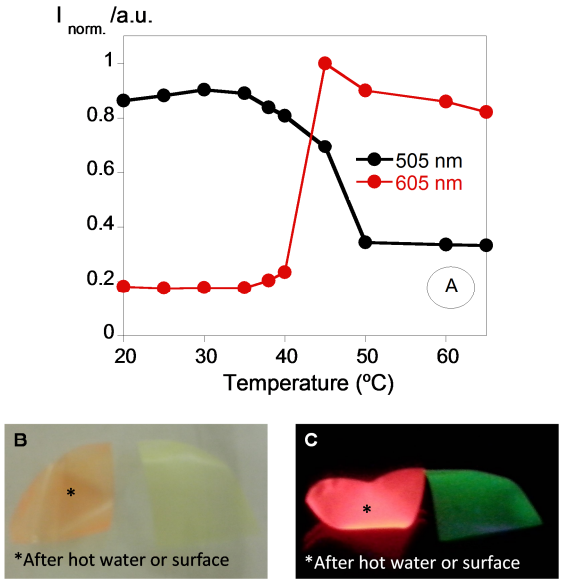

Figure 13. (A) Normalised emission as a function of temperature at 505 nm and 605 nm of polymethylmethacrylate (PMMA) doped with the complex $[Pt(pz^{R(10,10)py})_2]$ **b10** on a hot-plate. Images of PMMA10 after heating in hot water or in contact with a hot surface, taken with the naked-eye (B) and under a UV lamp (C) (λ_{exc} = 365 nm).

would alert us that the device or its battery could have been damaged by misuse, although the temperature returns to normal conditions.

Conclusions

Novel luminescent Pt(II) metallomesogens of the type $[Pt(pz^{R(n,n)py})_2]$ supported by dicatenar pyridylpyrazolate ligands have been synthesized and characterised. All complexes behave

as liquid crystal materials exhibiting hexagonal columnar mesophases (Col_h) with wide temperature ranges. However, the mesomorphic behaviour of these compounds shows a strong dependence with the alkyl chains length. The results suggest that when the core-core interactions predominate over the van der Waals ones (in complexes with n = 4-10), a columnar arrangement is favoured giving rise to stable mesophases with temperature intervals that exceed 150 ºC in some cases.

Several spectrophotometric and spectrofluorimetric titrations of the platinum complexes and their corresponding pyrazole ligands were performed in dichloromethane solutions. In particular, the addition of Hg^{2+} leads to the formation of the species with 2:1 ligand-to-metal or 1:1 complex-to-metal stoichiometries. In both cases, a CHEQ effect of the emission band was observed after titrations. In addition, ligands were also used as fluorescence probes to selective detection of Zn^{2+}, Cd^{2+} and Pd^{2+}.

Photoluminescent studies in the solid state at variable temperature show that the luminescent emission of the Pt(II)-bispyrazolate complexes is enhanced in the liquid-crystalline state. Furthermore, the emission band is significantly red-shifted with respect to that of the solid phase. This feature is explained on the basis of the formation of Pt–Pt interactions, which lead to the ^{3}MMLCT transition responsible for the luminescence observed. Taking advantage these properties we have constructed polymeric solid supports doped with the complex $[Pt(pz^{R(10,10)py})_2]$, which has been proved to be useful as temperature sensors for real technological applications.

In summary, the effectiveness of the *N,N*-bidentate coordination of the mesogenic ligands towards Pt metal centre has allowed to obtain new poly-functional liquid crystal and luminescent materials. The columnar supramolecular organisation of these new metallomesogens along with their attractive photophysical properties could be useful for designing novel devices which could contribute to develop more competent technologically materials.

Experimental section

Starting materials

K_2PtCl_4, $Hg(NO_3)_2\cdot xH_2O$, tetrakis(acetonitrile)palladium(II) tetrafluoroborate ($[Pd(CH_3CN)_4][BF_4]_2$), $Zn(BF_4)_2\cdot xH_2O$, polymethylmethacrylate (PMMA) compounds were purchased from Sigma-Aldrich and $Cd(CF_3SO_3)_2$ was obtained from Solchemar. All these chemicals were used without further purification. The 3-(3,5-bis(alkyloxy)phenyl)-(5-pyridin-2-yl)pyrazole ligands $[Hpz^{R(n,n)py}]$ **a4-a18** were prepared as we described in a previous work.[31]

Physical measurements

Elemental analyses for carbon, hydrogen and nitrogen were carried out by the Microanalytical Service of Complutense University (validated range: %C 0.5-94.7, %H 0.5-7.6, %N 0.5-23.0). IR spectra were recorded on a Perkin Elmer Spectrum 100 FTIR spectrophotometer with a universal ATR accessory in the 4000-650 cm^{-1} region: w (weak), m (medium) and s (strong). ^{1}H, ^{13}C NMR and DEPT spectra were performed at room temperature on a Bruker DPX-300 spectrophotometer (NMR Service of Complutense University) from solutions in $CDCl_3$. Chemical shifts δ are listed relative to Me_4Si using the signal of the deuterated solvent as a reference (7.26 and 77.0 ppm for ^{1}H and ^{13}C, respectively) and coupling constants J are in hertz. Multiplicities are indicated as s (singlet), d (doublet), t (triplet), q (quartet), quint (quintet), ddd (doublet of doublets of doublets), m (multiplet). The ^{1}H and ^{13}C chemical shifts are accurate to ±0.01 and ±0.1 ppm, respectively, and coupling constants to ±0.3 Hz.

Phase studies were carried out by optical microscopy using an Olympus BX50 microscope equipped with a Linkam THMS 600 heating stage. The temperatures were assigned on the basis of optic observations with polarised light. Measurements of the transition temperatures were made using a Perkin Elmer Pyris 1 differential scanning calorimeter with the sample (1 – 4 mg) sealed hermetically in aluminium pans and with a heating or cooling rate of 10 $Kmin^{-1}$. The X-ray diffractograms at variable temperature were recorded on a Panalytical X'Pert PRO MPD diffractometer with Cu-Kα (1.54 Å) radiation in a $\theta - \theta$ configuration equipped with an Anton Paar HTK1200 heating stage (X-Ray Diffraction Service of Complutense University).

Photophysical measurements

UV-Vis absorption spectra were recorded with a Jasco V-650 spectrophotometer equipped with a Julabo thermostat, and the luminescence emission by a Horiba J-Y Scientific Fluoromax-4 spectrofluorimeter. The linearity of the luminescence emission *vs*. concentration was checked in the concentration range used (10^{-5} – 10^{-6} M). A correction for the absorbed light was performed when necessary. The spectroscopic characterisations and titrations were performed using stock solutions of the compounds (*ca*. 10^{-3} M), prepared by dissolving the appropriate amount of **a6**, **a10**, **a12**, **a18**, **b4-b14**, **c6**, **c12**, **d6** and **d18** in dichloromethane in a 10 mL volumetric flask. The studied solutions were prepared by appropriate dilution of the stock solutions up to 10^{-5} – 10^{-6} M. Titrations were carried out by the addition of microliter amounts of standard solutions of the soft metal ions, Hg^{2+}, Pd^{2+}, Zn^{2+} and Cd^{2+} in dry acetonitrile.

All measurements were performed at 298 K. Luminescence quantum yields were measured using a solution of quinine sulfate in sulfuric acid (0.1 M) as a standard [Φ_F = 0.54][47,48] and were corrected for different refraction indexes of solvents. Lifetime measurement in degassed CH_2Cl_2 solution was recorded in a Tempro Fluorescence Lifetime System, from Horiba J-Y.

Luminescence spectra of solid samples were measured using a fibre optic system connected to the Horiba J-Y Fluoromax-4 spectrofluorimeter exciting at appropriate λ (nm) of the solid compounds. Lifetime measurement in the solid state under argon was recorded with a Horiba J-Y Fluoromax-4 spectrofluorimeter with a NanoLED pulsed laser.

Synthesis of the platinum complexes $[Pt(pz^{R(n,n)py})_2]$ b4-b18

A solution of K_2PtCl_4 (0.12 mmol, 0.05 g) in 5 mL of distilled water was added to a solution of the corresponding pyrazole $[Hpz^{R(n,n)py}]$ (0.24 mmol) in 15 mL of ethanol (96 %) under nitrogen atmosphere. The mixture was refluxed for 24 h and the deep-red residue obtained after cooling at room temperature was dissolved in 15 mL of $CHCl_3$ and then filtered over celite. Addition of acetone gave rise to red (n = 4-8) or yellow (n = 10-18) solids, which were filtered off and dried *in vacuo*. Finally, the first red complexes were converted to yellow crystals by slow

evaporation of a chloroform-acetone mixed solution of the corresponding complex.

[Pt(pz$^{R(4,4)py}$)$_2$] (b4): Yellow solid (40%). Found: C, 56.4 H, 5.5; N, 9.0. $PtC_{44}N_6H_{52}O_4 \cdot H_2O$ requires: C, 56.1; H, 5.7; N, 8.9%. ν_{max}/cm^{-1} 1597s ν(C=C + C=N), 764m γ(C-H)$_{py}$. δ_H (300 MHz; $CDCl_3$; Me_4Si): 0.99 (12H, t, ^3J 7.4, CH_3), 1.56 (8H, m, CH_2) 1.84 (8H, qt, ^3J 6.7, CH_2), 4.07 (8H, t, ^3J 6.7, OCH_2), 6.44 (2H, t, ^4J 2.2, H_p), 6.90 (2H, s, 4'-H), 7.10 (4H, d, ^4J 2.2, H_o), 7.26 (2H, m, 5-H), 7.63 (2H, d, ^3J 7.7, 3-H), 7.88 (2H, ddd, ^3J 7.6, 7.7, ^4J 1.3, 4-H), 10.83 (2H, d, ^3J 5.4, 6-H).

[Pt(pz$^{R(6,6)py}$)$_2$] (b6): Yellow solid (39%). Found: C, 60.0 H, 6.5; N, 8.1. $PtC_{52}N_6H_{68}O_4$ requires: C, 60.3; H, 6.6; N, 8.1%. ν_{max}/cm^{-1} 1594s ν(C=C + C=N), 765m γ(C-H)$_{py}$. δ_H (300 MHz; $CDCl_3$; Me_4Si): 0.94 (12H, t, ^3J 7.1, CH_3), 1.37 (16H, m, CH_2), 1.50 (8H, m, CH_2), 1.86 (8H, qt, ^3J 6.7, CH_2), 4.06 (8H, t, ^3J 6.6, OCH_2), 6.44 (2H, t, ^4J 2.2, H_p), 6.78 (2H, s, 4'-H), 7.04 (4H, d, ^4J 2.2, H_o), 7.13 (2H, ddd, ^3J 7.6, 5.4, ^4J 1.3, 5-H), 7.45 (2H, d, ^3J 7.7, 3-H), 7.72 (2H, ddd, ^3J 7.6, 7.7, ^4J 1.3, 4-H), 10.65 (2H, d, ^3J 5.4, 6-H).

[Pt(pz$^{R(8,8)py}$)$_2$] (b8): Yellow solid (35%). Found: C, 62.4 H, 7.4; N, 7.3. $PtC_{60}N_6H_{84}O_4$ requires: C, 62.7; H, 7.4; N, 7.3%. ν_{max}/cm^{-1} 1598s ν(C=C + C=N), 765m γ(C-H)$_{py}$. δ_H (300 MHz; $CDCl_3$; Me_4Si): 0.92 (12H, t, ^3J 7.1, CH_3), 1.34 (32H, m, CH_2), 1.54 (8H, m, CH_2), 1.84 (8H, qt, ^3J 6.7, CH_2), 4.06 (8H, t, ^3J 6.6, OCH_2), 6.44 (2H, t, ^4J 2.2, H_p), 6.78 (2H, s, 4'-H), 7.04 (4H, d, ^4J 2.2, H_o), 7.13 (2H, ddd, ^3J 7.6, 5.6, ^4J 1.3, 5-H), 7.55 (2H, d, ^3J 7.7, 3-H), 7.72 (2H, ddd, ^3J 7.6, 7.7, ^4J 1.3, 4-H), 10.75 (2H, d, ^3J 5.6, 6-H).

[Pt(pz$^{R(10,10)py}$)$_2$] (b10): Yellow solid (50%). Found: C, 63.0 H, 7.6; N, 6.7 %. $PtC_{68}N_6H_{100}O_4 \cdot 2H_2O$ requires: C, 63.0; H, 8.0; N, 6.5%. ν_{max}/cm^{-1} 1597s ν(C=C + C=N), 764m γ(C-H)$_{py}$. δ_H (300 MHz; $CDCl_3$; Me_4Si): 0.89 (12H, t, ^3J 6.9, CH_3), 1.28 (56H, m, CH_2), 1.85 (8H, qt, ^3J 6.6, CH_2), 4.05 (8H, t, ^3J 6.5, OCH_2), 6.43 (2H, t, ^4J 2.1, H_p), 6.77 (2H, s, 4'-H), 7.04 (4H, d, ^4J 2.1, H_o), 7.12 (2H, m, 5-H), 7.43 (2H, d, ^3J 7.8, 3-H), 7.77 (2H, m, 4-H), 10.63 (2H, d, ^3J 5.5, 6-H).

[Pt(pz$^{R(12,12)py}$)$_2$] (b12): Yellow solid (48%). Found: C, 65.5 H, 8.1; N, 6.1. $PtC_{76}N_6H_{116}O_4.H_2O$ requires: C, 65.6; H, 8.5; N, 6.0%. ν_{max}/cm^{-1} 1597s ν(C=C + C=N), 763m γ(C-H)$_{py}$. δ_H (300 MHz; $CDCl_3$; Me_4Si): 0.87 (12H, t, ^3J 6.9, CH_3), 1.26 (72H, m, CH_2), 1.84 (8H, qt, ^3J 6.5, CH_2), 4.06 (8H, t, ^3J 6.5, OCH_2), 6.43 (2H, t, ^4J 2.1, H_p), 6.83 (2H, s, 4'-H), 7.06 (4H, d, ^4J 2.1, H_o), 7.18 (2H, m, 5-H), 7.52 (2H, d, ^3J 7.8, 3-H), 7.79 (2H, m, 4-H), 10.73 (2H, d, ^3J 5.5, 6-H). δ_c (75.48 MHz; $CDCl_3$; Me_4Si): 14.1 (CH_3), 22.7 (CH_2), 26.2 (CH_2), 29.3 (CH_2), 29.4 (CH_2), 29.5 (CH_2), 29.6 (CH_2), 29.7 (CH_2), 31.9 (CH_2), 68.0 (OCH_2), 99.5 (C-4'), 100.2 (C_P), 103.7 (C_o), 117.8 (C-3), 120.4 (C-5), 136.8 (C_i), 138.2 (C-4), 149.5 (C-3'), 150.4 (C-2), 151.3 (C-6), 154.0 (C-5'), 160.3 (C_m).

[Pt(pz$^{R(14,14)py}$)$_2$] (b14): Yellow solid (40%). Found: C, 67.9 H, 8.8; N, 5.7. $PtC_{84}N_6H_{132}O_4$ requires: C, 67.9; H, 8.9; N, 5.7%. ν_{max}/cm^{-1} 1598s ν(C=C + C=N), 766m γ(C-H)$_{py}$. δ_H (300 MHz; $CDCl_3$; Me_4Si): 0.87 (12H, t, ^3J 6.9, CH_3), 1.26 (88H, m, CH_2), 1.84 (8H, qt, ^3J 6.7, CH_2), 4.05 (8H, t, ^3J 6.6, OCH_2), 6.43 (2H, t ^4J 2.1, H_p), 6.86 (2H, s, 4'-H), 7.07 (4H, d, ^4J 2.1, H_o), 7.24 (2H, m, 5-H), 7.55 (2H, d, ^3J 7.9, 3-H), 7.83 (2H, m, 4-H), 10.75 (2H, d, ^3J 5.6, 6-H).

[Pt(pz$^{R(16,16)py}$)$_2$] (b16): Yellow solid (44%). Found: C, 68.4 H, 9.0; N, 5.2. $PtC_{92}N_6H_{148}O_4.H_2O$ requires: C, 68.4; H, 9.3; N, 5.2%. ν_{max}/cm^{-1} 1598s ν(C=C + C=N), 765m γ(C-H)$_{py}$. δ_H (300 MHz; $CDCl_3$; Me_4Si): 0.87 (12H, t, ^3J 6.8, CH_3), 1.26 (104, m, CH_2), 1.84 (8H, qt, ^3J 6.6, CH_2), 4.05 (8H, t, ^3J 6.5, OCH_2), 6.43 (2H, t, ^4J 2.1, 5-H), 6.89 (2H, s, 4'-H), 7.09 (4H, d, ^4J 2.1, H_o), 7.26 (2H, m, 5-H), 7.59 (2H, d, ^3J 7.6, 3-H), 7.86 (2H, m, 4-H), 10.81 (2H, d, ^3J 5.7, 6-H).

[Pt(pz$^{R(18,18)py}$)$_2$] (b18): Yellow solid (38%). Found: C, 70.2 H, 9.2; N, 4.9. $PtC_{100}N_6H_{164}O_4$ requires: C, 70.3; H, 9.6; N, 4.9%. ν_{max}/cm^{-1} 1597s ν(C=C + C=N), 765m γ(C-H)$_{py}$. δ_H (300 MHz; $CDCl_3$; Me_4Si): 0.87 (12H, t, ^3J 6.9 Hz, CH_3), 1.25 (120H, m, CH_2), 1.84 (8H, qt, ^3J 6.7, CH_2), 4.05 (8H, t, ^3J 6.6, OCH_2), 6.43 (2H, t, ^4J 2.2, H_p), 6.89 (2H, s, 4'-H), 7.10 (4H, d, ^4J 2.2, H_o), 7.26 (2H, m, 5-H), 7.62 (2H, d, ^3J 7.6, 3-H), 7.88 (2H, m, 4-H), 10.85 (2H, d, ^3J 5.5 6-H).

DFT calculation method

DFT and TDDFT calculations were run with Gaussian09[46] with default grids and convergence criteria. The input geometry for the parallel-displaced conformation was obtained from the X-ray geometry, whereas the input geometry for the sandwich conformation was obtained by sliding one complex from the previous conformation along the aromatic plane, as to place the platinum atoms above each other. The hydrogen positions of both conformations were optimized prior to the calculation of the TD spectra, with all remaining atoms fixed at their initial positions. All calculations were performed using the B3LYP functional and the LanL2DZ basis set, consisting of a D95V set for hydrogen and first-row elements, and a Los Alamos effective core potential (ECP) plus a DZ set for the valence electrons of Pt. Vertical excitations energies and oscillator strengths were solved for the first 10 singlet excited states using the formalism implemented in Gaussian09.[49-53]

Table 6. Crystal and refinement data for **b8**

Empirical formula	$[C_{60}H_{84}N_6O_4Pt]$
Formula weight	1148.42
Crystal system	Triclinic
Space group	*P*(-1)
Space group number	2
a / Å	6.7075(8)
b / Å	17.804(2)
c / Å	24.778(3)
α (º)	79.629(2)
β (º)	85.170(2)
γ (º)	83.157(3)
V / Å^3	2883.9(6)
Z	2
T / K	296(2)
F(000)	1192
ρ_c / g cm^{-3}	1.322
μ / mm^{-1}	2.482
Scan technique	ω and φ
Data collected	(-7, -21, -24) to (7, 20, 29)
θ range (º)	1.17 to 25.00
Reflections collected	22107
Independent reflections	9850 (R_{int} = 0.0900)
Completeness to maximum θ (%)	97.4
Data / restraints / parameters	9850 / 0 / 640
Observed reflections [$I > 2\sigma(I)$]	4874
R^a	0.0608
$R_{wF}{}^b$	0.1687

^{a} $\Sigma[|F_o| - |F_c|] / \Sigma[|F_o|]$. ^{b} $\{\Sigma[w(F_o^2 - F_c^2)^2] / \Sigma[w(F_o^2)^2]\}^{1/2}$

Preparation of the solid support doped with compound [Pt(pz$^{R(10,10)py}$)$_2$] b10

A solid support based on polymethylmethacrylate (PMMA) was prepared by dissolving 100 mg of PMMA powder in dichloromethane, followed by the addition of compound **b10** (5 mg) dissolved in the same solvent. The polymer film was obtained after very slow evaporation at room temperature (~ 48 hours).

X-ray crystal structure determination

Data collection of [Pt(pz$^{R(8,8)py}$)$_2$] **b8** was carried out at room temperature on a Bruker Smart CCD diffractometer using graphite-monochromated Mo-Kα radiation (λ = 0.71073 Å) operating at 50 kV and 35 mA. The data were collected over a hemisphere of the reciprocal space by combination of three exposure sets. Each exposure of 20 s covered 0.3º in ω. The cell parameters were determined and refined by a least-squares fit of all reflections. The first 100 frames were recollected at the end of the data collection to monitor crystal decay, and no appreciable decay was observed. Empirical absorption corrections were made using SADABS program.[54] A summary of the fundamental crystal and refinement data is given in Table 6.

The structure was solved by direct methods and refined by full-matrix least-square procedures on F^2 (SHELXL-97).[55] All non-hydrogen atoms were refined anisotropically. The hydrogen atoms were included in their calculated positions and refined riding on their respective carbon atoms.

CCDC 1008267 contains the supplementary crystallographic data for this paper. These data can be obtained free of charge from The Cambridge Crystallographic Data Centre via www.ccdc.cam.ac.uk/data_request/cif.

Acknowledgment

M. Cano is grateful to the Ministerio de Economía y Competitividad (Spain), project CTQ2011-25172. E. Oliveira acknowledges the post-doctoral grant from *Fundação para a Ciência e a Tecnologia* (Portugal) SFRH/BPD/72557/2010. PROTEOMASS Scientific Society (Portugal) and PROTEOMASS Scientific Society (Spain) are also acknowledged for funding. C. Lodeiro thanks to REQUIMTE-FCT PEst-C/EQB/LA0006/2013 for funding. We would like to thank Prof. Guillermo Orellana and Dra. Ana Belén Descalzo for their contribution and help with the lifetime measurement.

Notes and references

[a] *Departamento de Química Inorgánica I, Facultad de Ciencias Químicas, Universidad Complutense, E-28040 Madrid, Spain. Fax: +34 91394 4352; Tel: +34 91394 4340; E-mail: mmcano@ucm.es.*
[b] *Laboratorio de Difracción de Rayos-X, Facultad de Ciencias Químicas, Universidad Complutense, E-28040 Madrid, Spain.*
[c] *BIOSCOPE Group, REQUIMTE, Chemistry Department, Faculty of Science and Technology, University NOVA of Lisbon 2829-516 Monte da Caparica, Portugal. Fax: 351 2129 48550; Tel: +351 2129 11402; E-mail: cle@fct.unl.pt.*
[d] *ProteoMass Scientific Society, Rua dos Inventores, Madan Park, 2825-182 Caparica, Portugal.*
[e] *Department of Chemistry and CICECO, University of Aveiro, Campus de Santiago, 3810-193 Aveiro, Portugal.*

† Electronic Supplementary Information (ESI) available: Selected bond distances and angles for complex **b8**, packing of **b8** in the *bc* plane, powder 2D XRD diffraction pattern for **b12** on heating, absorption spectra titrations for **a18** in CH_2Cl_2 solution, fluorescence spectra of compound **a6** in solid state as a function of temperature, DFT simulated parallel-displaced and sandwich conformations and X-ray crystallographic files for **b8** (CIF). See DOI: 10.1039/b000000x/

‡ Molecular volume: $V_{mol} = M_w/(N_A \cdot \rho)$; where M_w is the molecular weight, N_A is Avogadro's number and ρ is the density (~ 1 g·cm^{-3}). Columnar cross-section area $S_{col} = (\sqrt{3})a^2/2$. Hexagonal lattice constant $a = \Sigma d_{hk}\sqrt{(h^2 + k^2 + hk)}/\sqrt{(3N_{hk})}$, where N_{hk} is the number of *hk0* reflections.

1 U. C. Spichiger-Keller, *Chemical Sensors and Biosensors for Medical and Biological Applications*, Wiley-VCH: Weinheim, Germany, 1998.
2 H. He, K. Jenkins, C. Lin, *Anal. Chim. Acta*, 2008, **611**, 197.
3 Haas, K. L.; Franz, K. J. *Chem. Rev.*, 2009, **109**, 4921.
4 S. Park, W. Kim, K. M. K. Swamy, H. Y. Lee, J. Y. Jung, G. Kim, S.-J. Kim, J. Yoon, *Dyes Pigments*, 2013, **99**, 323.
5 F. Yang, M. Wang, D. Cao, N. Yang, Y. Fu, L. Chen, *Dyes Pigments* 2013, **98**, 42.
6 R. Y. Tsien, in *Fluorescent and Photochemical Probes of Dynamic Biochemical Signals inside Living Cells*, ed. A. W. Czarnik, American Chemical Society, Washington, DC, 1993, pp. 130-146.
7 X. Guo, X. Qian, L. Jia, *J. Am. Chem. Soc.*, 2004, **126**, 2272.
8 C. Núñez, M. Diniz, A. A. D. Santos, J. L. Capelo, C. Lodeiro, *Dyes Pigments*, 2014, **101**, 156.
9 Q. Li, M. Peng, N. Li, J. Quin, Z. Li, *Sensors Actuat. B-Chem.*, 2012, **173**, 580.
10 X. M. Meng, L. Liu, Q. X. Guo, *Progr. Chem.*, 2005, **17**, 45.
11 W. P. Zhu, Y. F. Xu, X. H. Quian, *Progr. Chem.*, 2007, **19**, 1229.
12 Z. Xu, J. Yoon, D. R. Spring, *Chem. Soc. Rev.*, 2010, **39**, 1996.
13 N. E. Okoronkwo, J. C. Igwe, I. J. Okoronkwo, *Afr. J. Biotechnol.*, 2007, **6**, 335.
14 F. Vera, J. L. Serrano, T. Sierra, *Chem. Soc. Rev.*, 2009, **38**, 781.
15 B. R. Kaafarani, *Chem. Mater.*, 2011, **23**, 378.
16 O. Kasdorf, J. Vollbrecht, B. Ohms, U. Hilleringmann, H. Bock, H.-S. Kitzerow, *Int. J. Energy Res.*, 2014, **38**, 452.
17 Q. Zheng, G. Fang, W. Bai, N. Sun, P. Qin, X. Fan, F. Cheng, L. Yuan, X. Zhao, *Sol. Energ. Mat. Sol. C.*, 2011, **95**, 2200.
18 C. E. Conn, V. Panchqnula, A. Weerawardena, L. J. Waddington, D. F. Kenedy, C. J. Drummond *Langmuir*, 2010, **26**, 6240.
19 V. H. Houlding, V. M. Miskowski, *Coord. Chem. Rev.*, 1991, **111**, 145.
20 D. R. McMillin, J. J. Moore, *Coord. Chem. Rev.*, 2002, **229**, 113.
21 J. S. Field, C. R. Wilson, O. Q. Munro, *Inorg. Chim. Acta*, 2011, **374**, 197.
22 Y. Abe, Y. Takagi, M. Nakamura, T. Takeuchi, T. Tanase, M. Yokokawa, H. Mukai, T. Megumi, A. Hachisuga, K. Ohta, *Inorg. Chim. Acta*, 2012, **392**, 254.
23 K. Venkatesan, P. H. J. Kouwer, S. Yagi, P. Müller, T. M. Swager, *J. Mater. Chem.*, 2008, **18**, 400.
24 M. Krikorian, S. Liu, T. M. Swager, *J. Am. Chem. Soc.*, 2014, **136**, 2952.
25 T. Hegmann, J. Kain, S. Diele, B. Schubert, H. Bögel, C. Tschierske, *J. Mater. Chem.*, 2003, **13**, 991.
26 C. Damm, G. Israel, T. Hegmann, C. Tschierske, *J. Mater. Chem.*, 2006, **16**, 1808.
27. B. Bilgin-Eran, H. Ocak, C. Tschierske, U. Baumeister, *Liq. Cryst.*, 2012, **39**, 467.
28 C. Cuerva, P. Ovejero, J. A. Campo, M. Cano, *New J. Chem.*, 2014, **38**, 511.
29 P. Ovejero, E. Asensio, J. V. Heras, J. A. Campo, M. Cano, M. R. Torres, C. Núñez, C. Lodeiro, *Dalton Trans.*, 2013, **42**, 2107.
30 L. Soria, P. Ovejero, M. Cano, J. A. Campo, M. R. Torres, C. Nuñez, C. Lodeiro, *Dyes Pigments*, 2014, **110**, 159.
31 C. Cuerva, J. A. Campo, P. Ovejero, M. R. Torres, M. Cano, *Dalton Trans.*, 2014, **43**, 8849.
32 V. R. R. Kumar, R. Mukhopadhyay, T. Pradeep, *J. Chem. Sci.*, 2008, **120**, 537.
33 S. Chandrasekhar, in *Liquid crystals of disklike molecules*, ed. G. H. Brown, Advances in Liquid Crystals, Elsevier, 1982, **5**, 47.
34 C.-W. Chien, K.-T. Liu, C. K. Lai, *J. Mater. Chem.*, 2003, **13**, 1588.

35 *International Tables for Crystallography*, *Vol. A*, 4th ed.; Hahn, T., Ed.; International Union of Crystallography; Kluwer Academic: Dordrecht, The Netherlands, 1995.

36 E. Cavero, S. Uriel, P. Romero, J. L. Serrano, R. Giménez, *J. Am. Chem. Soc.*, 2007, **129**, 11608.

37 E. M. Nolan, S. J. Lippard, *Chem. Rev.*, 2008, **108**, 3443.

38 A. Tamayo, B. Pedras, C. Lodeiro, L. Escriche, J. Casabó, J. L. Capelo, B. Covelo, R. Kivekäs, R. Sillanpä, *Inorg. Chem.*, 2007, **46**, 7818.

39 M. Mameli, V. Lippolis, C. Caltagirone, J. L. Capelo, O. Nieto, C. Lodeiro, *Inorg. Chem.*, 2010, **49**, 8276.

40 P. Gans, A. Sabatini, A. Vacca, *Talanta*, 1996, **43**, 1739.

41 P. MacCarthy, *Anal. Chem*., 1978, **50**, 2165.

42 C.-T. Liao, H-H. Chen, H-F. Hsu, A. Polock, H-H. Yeh, Y. Chi, K-W. Wang, C-H. Lai, G.-H. Lee, C-W. Shih, P-T. Chou, *Chem. Eur. J*., 2011, **17**, 546.

43 P-T. Chou, Y. Chi, *Chem. Eur. J*. 2007, **13**, 380.

44 M. Mydlak, M. Mauro, F. Polo, M. Felicetti, J. Leonhardt, G. Diener, L. De Cola, C. A. Strassert, *Chem. Mater*., 2011, **23**, 3659.

45 D. Kim, J-L. Brédas, *J. Am. Chem.*, 2009, **131**, 11371.

46 Gaussian 09, Revision A.02, Gaussian, Inc: Wallingford CT, 2009.

47 I. B. Berlman, *Handbook of Fluorescence Spectra of Aromatic Molecules*, 2nd Ed., Academic Press: New York, 1971.

48 M. Montalti, A. Credi, L. Prodi, M. T. Gandolfi, *Handbook of Photochemistry*, 3rd Ed., Taylor & Francis: Boca Raton, 2006.

49 R. Bauernschmitt, R. Ahlrichs, *Chem. Phys. Lett.*, 1956, **256** 454.

50 R. E. Stratmann, G. E. Scuseria, M. J. Frisch, *J. Chem. Phys*., 1998, **109**, 8218.

51 (a) C. Van Caillie, R. D. Amos, *Chem. Phys. Lett*., 1999, **308** 249. (b) C. Van Caillie, R. D. Amos, *Chem. Phys. Lett*., 2000, **317**, 159.

52 F. Furche, R. Ahlrichs, *J. Chem. Phys.*, 2002, **117**, 7433.

53 G. Scalmani, M. J. Frisch, B. Mennucci, J. Tomasi, R. Cammi, V. Barone, *J. Chem. Phys*, 2006, **124**, 1.

54 G. M. Sheldrick, *SADABS, Program for Absorption Corrections Using Bruker CCD Data*, University of Göttingen, Germany, 2001.

55 G. M. Sheldrick, *SHELX97, Program for Refinement of Crystal Structure*, University of Göttingen: Germany, 1997.

Columnar discotic Pt(II) metallomesogens as luminescence multifunctional materials with chemo and thermosensor abilities.

Cristián Cuerva[a], José A. Campo[a], Paloma Ovejero[a], M. Rosario Torres[b], Elisabete Oliveira[c,d], Sérgio M. Santos[e], Carlos Lodeiro[*c,d] and Mercedes Cano[*a]